Int. J. Bio-Inorg. Hybd. Nanomat., Vol. 1, No. 1 (2012), 7-15 *ISSN: 2251-8533*

International Journal of Bio-Inorganic Hybrid Nanomaterials

Hydrothermal Synthesis of New $Ln_xSb_{2-x}S_3$ ($Ln: Yb^{3+}, Er^{3+}$) Nanomaterials and Investigation of Physical Properties

Abdolali Alemi[1*], Younes Hanifehpour[1,2], Sang Woo Joo[2], Bong-Ki Min[3]**

[1] Department of Inorganic Chemistry, Faculty of Chemistry, University of Tabriz, Iran
[2] School of Mechanical Engineering, WCU Nano Research Center, Yeungnam University, Gyongsan 712-749 South Korea
[3] Center for Research Facilities, Yeungnam University, Gyongsan, South Korea

Received: 3 December 2011; Accepted: 2 February 2012

ABSTRACT

$Ln_xSb_{2-x}S_3$ (Ln: Yb^{3+}, Er^3) based nanomaterials were synthesized by a co-reduction method. Powder XRD patterns indicate that the $Ln_xSb_{2-x}S_3$ crystals (Ln = Yb^{3+}, Er^{3+}, x = 0.00-0.09) are isostructural with Sb_2S_3. The cell parameter a and c increase for Ln = Er^{3+} and Yb^{3+} upon increasing the dopant content (x), while b decreases. SEM images show that doping of the lanthanide ions in the lattice of Sb_2S_3 result in nanoflowers and nanoparticles. Emission spectra of Yb^{3+} doped materials, in addition to the characteristic red emission peaks of Sb_2S_3 emission, show other bands originating very probably from the $^2F_{5/2} \rightarrow {}^2F_{7/2}$ in case of Yb^{3+} doped crystals.The electrical conductance of Ln-doped Sb_2S_3 is higher than pure Sb_2S_3 and increase with temperature.

Keyword: Nanoflower; Luminescence; Electrical Conductance; Hydrothermal.

1. INTRODUCTION

Ln^{3+}-doped inorganic nanocrystals with various compositions have become an increasingly important research topic, and opened up the opportunity for creating new applications in diverse areas, such as light emitting displays, biological labelling and imaging, owing to their distinct electrical and optical properties [1-3]. Antimony sulfide, a layer-structured direct band gap semiconductor with orthorhombic crystal structure, is an important semiconductor with high photosensitivity and thermoelectric power [4]. Due to its good photo-conductivity, Sb_2S_3 has received significant

(*) Corresponding Author - e-mail: Alemi@Tabrizu.ac.ir
(**) e-mail: swjoo@yu.ac.kr

attention for potential applications in solar energy conversion [5]. It has also been used in switching devices [6], thermoelectric cooling technologies, optoelectronics in the IR region [7,8], and microwave devices [9], television cameras [10]. Over the past two decades, many methods have been employed to prepare Sb_2S_3 nanotubes, nanowires, nanorods, nanobelts, and nanospheres, including thermal decomposition [11], hydrothermal reaction [12,13], microwave irritation [14], and vacuum evaporation [5]. Studies of impurity effects or doping agents on the physical properties of Sb_2Se_3 are interesting both for basic and applied research. Doping of trivalent cations such as Sb^{3+} [15], In^{3+} [16], Fe^{3+} [17], Mn^{3+} [18], and a number of further trivalent 3d elements [19] to the lattice of Bi_2Se_3 have been investigated, also EPR spectra of Gd-doped bulk Bi_2Se_3 [20]. Also, New $Ln_xBi_{2-x}Se_3$ (Ln: Sm^{3+}, Eu^{3+}, Gd^{3+}, Tb^{3+}, Nd^{3+}) based nanomaterials were synthesized by Alemi and et al [21, 22]. Recently, we have reported novel luminescent nanomaterials based on doping of Lanthanide (Ln: Ho^{3+}, Nd^{3+}, Lu^{3+}) into the lattice of Sb_2S_3 and (Ln: Ho^{3+}, Nd^{3+}, Lu^{3+}, Sm^{3+} ,Er^{3+}, Yb^{3+}) into the lattice of Sb_2Se_3 [23-26]. The incorporation of large electropositive ions such as lanthanides into antimony chalcogenide frameworks is expected to lead to materials with various properties. The incorporation of lanthanide ions into a Sb-S framework could dramatically affect the electronic properties of that framework. In this study synthesis of $Sb_{2-x}ln_xS_3$ (ln: Yb^3, Er^{3+}) nanocrystals by a hydrothermal route is described. Nanomaterials of Sb_2S_3 were synthesized by introducing small amounts of Yb^{3+} and Er^{3+} to the Sb_2S_3 lattice. Structural, spectroscopic properties and electrical conductance of the synthesized materials are reported.

2. EXPERIMENTAL

Materials and methods

All chemicals were of analytical grade, and were used without further purification. Sulfur powder (0.032 g, 1 mmol) and NaOH (0.6 g, 15 mmol) were added to distilled water (60 mL), and stirred well for 10 min at room temperature. Afterwards, hydrazinium hydroxide (2 mL, 40 mmol) and $SbCl_3$ (2, 1.96, 1.94, 1.91 mmol), and Ln_2O_3 (ln:Yb, Er) (0.00, 0.04, 0.06, 0.09 mmol) were added, and the mixture was transferred to a 100 mL Teflon-lined autoclave. The autoclave was sealed, maintained at 180°C for 48 h, and then cooled to room temperature. The black precipitate obtained was filtered and washed with ethanol and water. It wasthen dried at room temperature. Yields for the products were 90-95 %. Elemental analysis gave C, H and N contents of below 0.1%. Phase identification was performed with an X-ray powder diffractometer (XRD D5000 Siemens) with Cu-K_α radiation. The morphology of the materials was examined using a JEOL JSM-6700F Scanning Electron Microscope. Elemental analyses were carried out using a linked ISIS-300, Oxford EDS (energy dispersion spectroscopy) detector. The samples were coated with gold powder before SEM and EDS measurements. The HRTEM image and SAED pattern were recorded by a Cs-corrected high-resolution TEM (JEM-2200FS, JEOL) operated at 200 kV. Photoluminescence measurements were carried out using a Spex FluoroMax-3 spectrometer after dispersing a trace amount of sample via ultrasound in distilled water. Cell parameters were calculated with Celref program from powder XRD patterns, and reflections have been determined and fitted using a profile fitting procedure with the Winxpow program. The reflections observed in 2θ = 4-70° were used for the lattice parameter determination.

3. RESULTS AND DISCUSSION

$Sb_{2-x}ln_xS_3$ (ln: Yb^{3+}, Er^{3+}) samples were prepared by a hydrothermal co--reduction method. The powder X-ray diffraction (P-XRD) patterns (see Figure 1) indicate that the Yb^{3+}-doped powders have the same orthorhombic structure as Sb_2S_3 and that single phase Sb_2S_3 is retained at lower doping concentrations of Ln^{3+}. All the peaks in the Figure 1 can be attributed to the orthorhombic phase of Sb_2S_3 with lattice parameters a=11.22 Å, b=11.28 Å

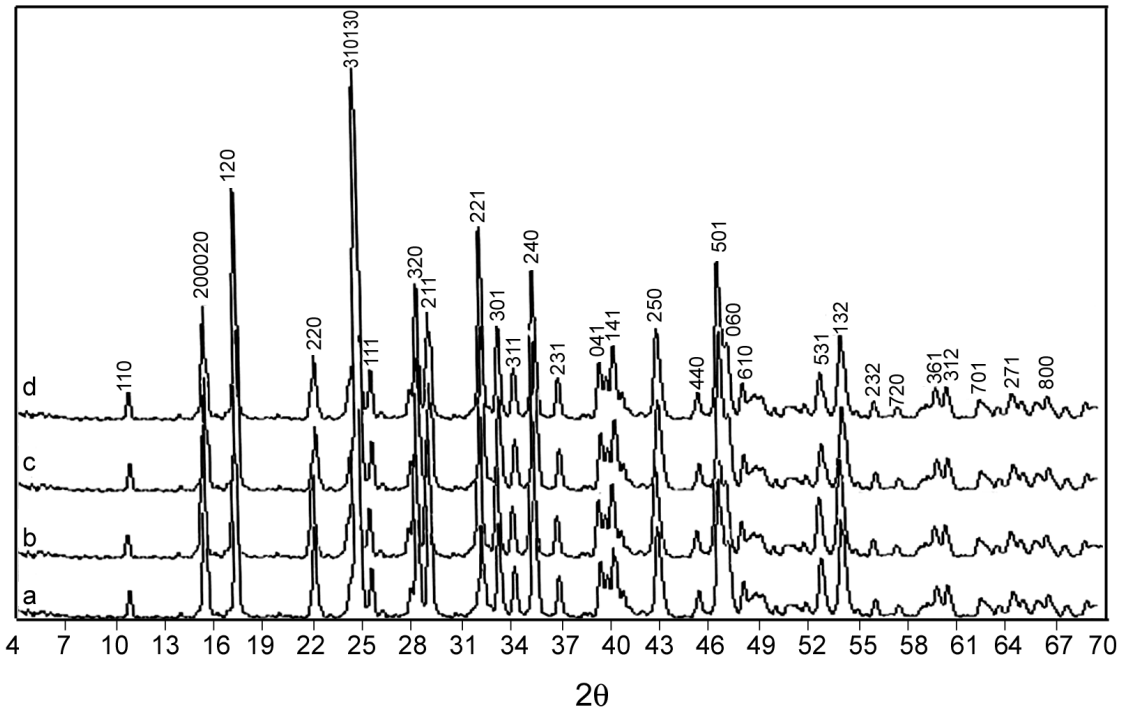

Figure 1: *Powder X-ray diffraction patterns of $Sb_{2-x}Yb_xSe_3$ (a: x = 0.0, b: x = 0.03, c: x = 0.06, d: x = 0.09) synthesized at 180°C and 48 h.*

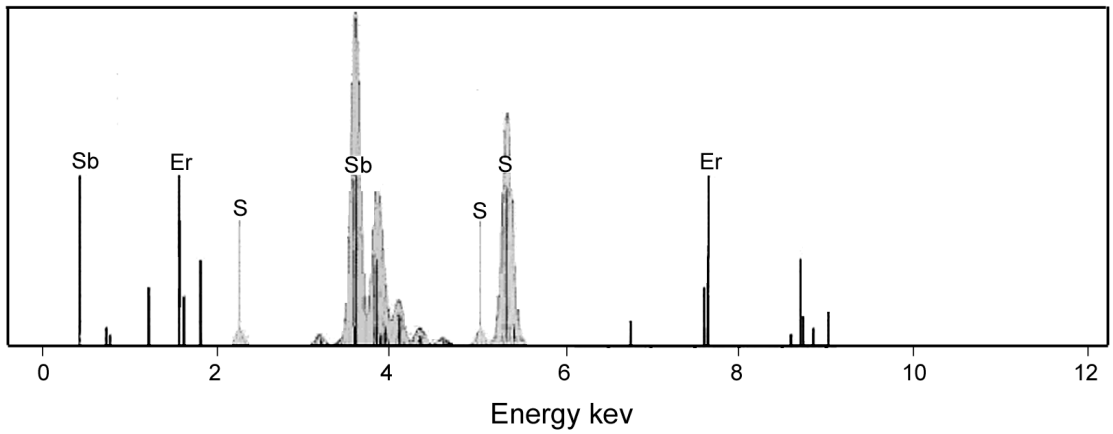

Figure 2: *EDX patterns of $Sb_{2-x}Er_xS_3$.*

and c=3.84 Å (JCPDS card File: 42-1393). In case of Er-doped Sb_2S_3, the intensity of some peaks are changed .Beyond doping levels of x = 0.09 for Yb^{3+} and Er^{3+} additional unknown phases were observed.

The EDX analysis of the product confirms the ratio of Sb/S/Er as expected (Figure 2). Also, ICP analysis confirms the exact amount of doping.

The cell parameters of the synthesized materials were calculated from the XRD patterns. With increasing dopant content (x), the a and c parameter for Yb^{3+} and Er^{3+} increases, while the b parameter

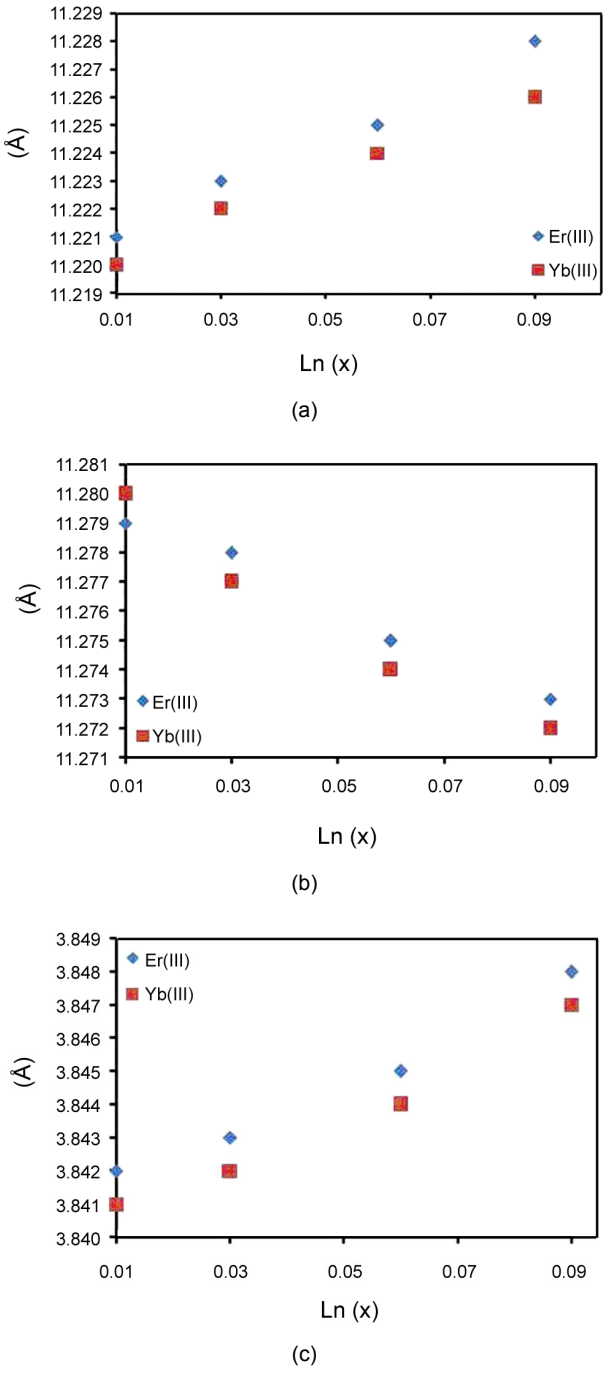

Figure 3: *The lattice constant of $Sb_{2-x}Ln_xS_3$ (x = 0 to 0.09) dependent upon Ln^{3+} doping on Sb^{3+} sites.*

decreases (Figure 3). The trend for lattice constants can be correlated to the effective ionic radii of the Ln^{3+} ions, assuming that the radius of Er^{3+} is larger than that of Yb^{3+}, which results in greater amount of lattice parameters for Er^{3+} doped materials.

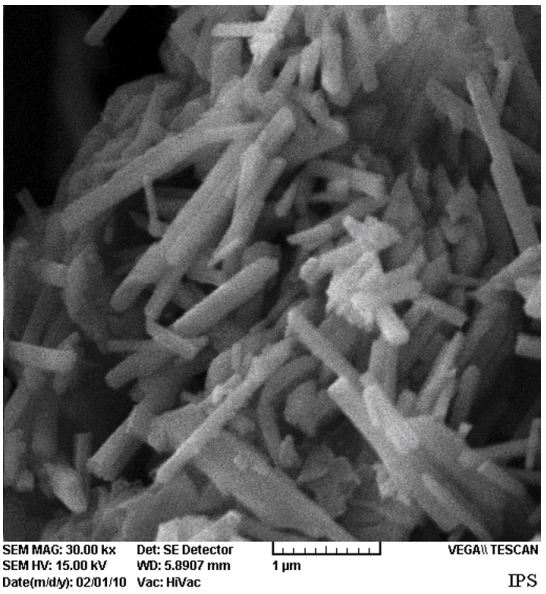

Fiure 4: *SEM image of Sb_2S_3 nanorods synthesized at 180°C and 48h.*

Scanning electron microscopic (SEM) images of Sb_2Se_3 nanorods are shown in Figures 4. Rods of about 4 µm lengths and thicknesses of 20-110 nm are observed for Sb_2Se_3.

Doping Yb^{3+} into the structure of Sb_2S_3 changes the morphology from rods to flowers. The thickness of the sheets in case of $Sb_{1.91}Yb_{0.09}S_3$ is less than 25 nm (Figure 5). The average diameter of the created pores in this morphology was estimated to be about 200 nm.

Figure 5: *SEM image of $Sb_{1.91}Yb_{0.09}S_3$ nanoflowers synthesized at 180°C and 48 h.*

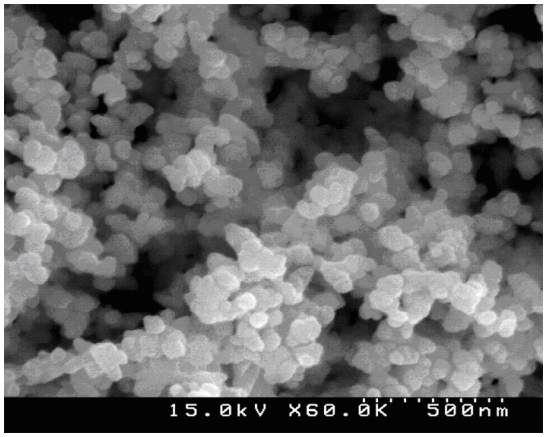

Figure 6: *SEM image of $Sb_{1.91}Er_{0.09}S_3$ nanoparticles synthesized at 180°C and 48 h.*

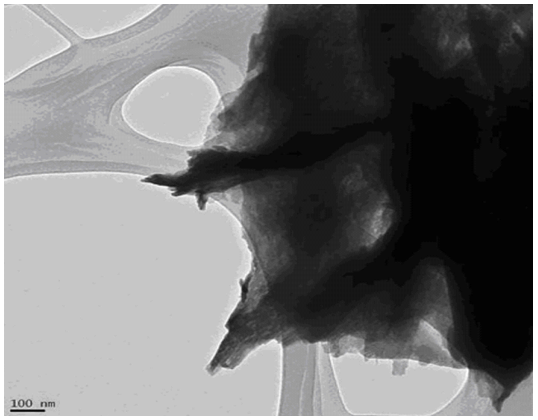

(a)

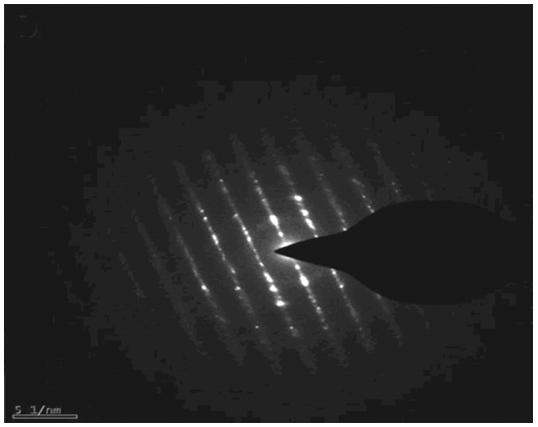

(b)

Figure 7: *TEM image and SAED pattern of $Sb_{1.91}Yb_{0.09}S_3$ nanoflowers synthesized at 180°C and 48 h.*

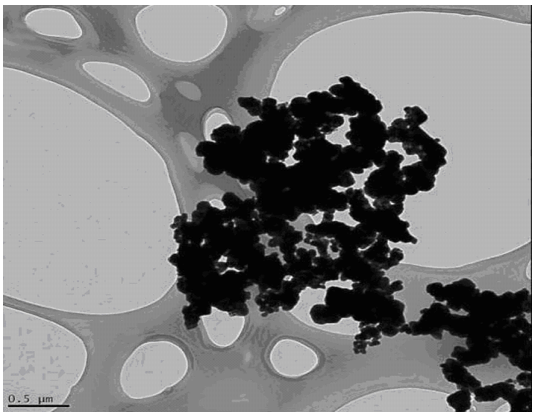

(a)

(b)

Figure 8: *TEM image and SAED pattern of $Sb_{1.91}Er_{0.09}S_3$ nanoparticles synthesized at 180°C and 48 h.*

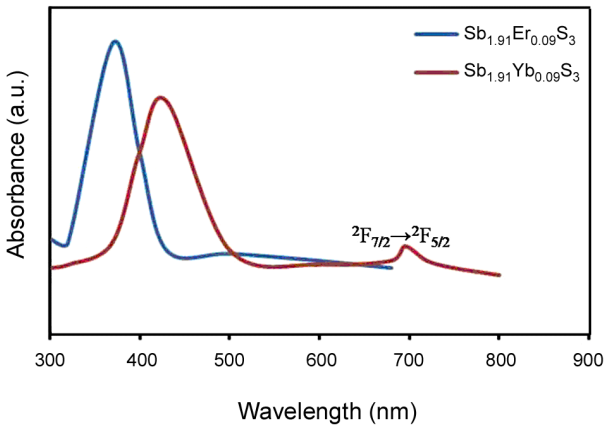

Figure 9: *Absorption spectra of $Sb_{1.91}Yb_{0.09}S_3$ and $Sb_{1.91}Er_{0.09}S_3$.*

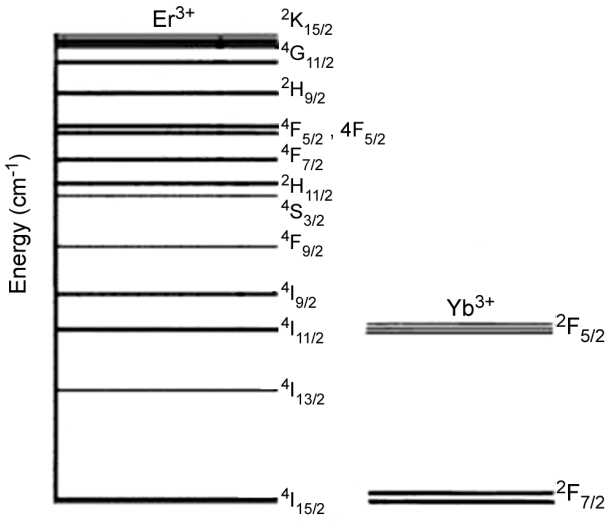

Figure 10: *Energy level diagrams of Yb^{3+} and Er^{3+} ions.*

Also, doping of Er^{3+} into the structure of Sb_2S_3 changes the morphology from rods to particles (Figure 6). The average diameter of $Sb_{1.91}Er_{0.09}S_3$ particles was estimated to be about 50 nm.

The TEM images obtained in ethanol/water media show that the $Sb_{1.91}Yb_{0.09}S_3$ flowers are uniform and confirm the result of SEM images (Figure 7a). The surface diameter of sheets in $Sb_{1.91}Yb_{0.09}S_3$ is 650 nm. Figure 7b shows SAED pattern and crystalinity of nanoflowers.

Figure 8a and b shows TEM image and SAED patterns of $Sb_{1.91}Yb_{0.09}S_3$ nanoparticles obtained in ethanol/water media that confirms the result through SEM images.

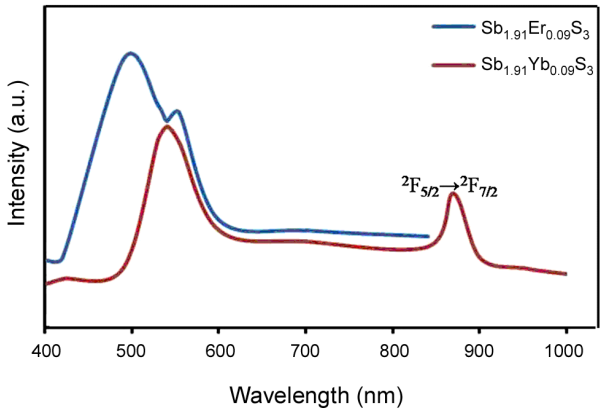

Figure 11: *Emission spectra for Sb_2S_3: Yb^{3+} and Sb_2S_3: Er^{3+} at RT.*

The absorption spectra of $Sb_{1.91}Yb_{0.09}S_3$ and $Sb_{1.91}Yb_{0.09}S_3$ crystals in the UV-Vis and near-IR region of 190-1000 nm are shown in Figure 9. Absorption spectra reveal the existence of Sb_2S_3 (in the near-UV) and Yb^{3+} ions in near-IR domain. For $Sb_{1.91}Yb_{0.09}S_3$ transition of the Er^{3+} ions are not observed because of instrument limitation. There is a red shift in doped materials in comparison to pure Sb_2S_3 .

These spectra are characterized by a small band in near-IR spectral domain, corresponding to the $^2F_{7/2} \rightarrow {}^2F_{5/2}$ transition (f-f transitions) of the Yb^{3+}

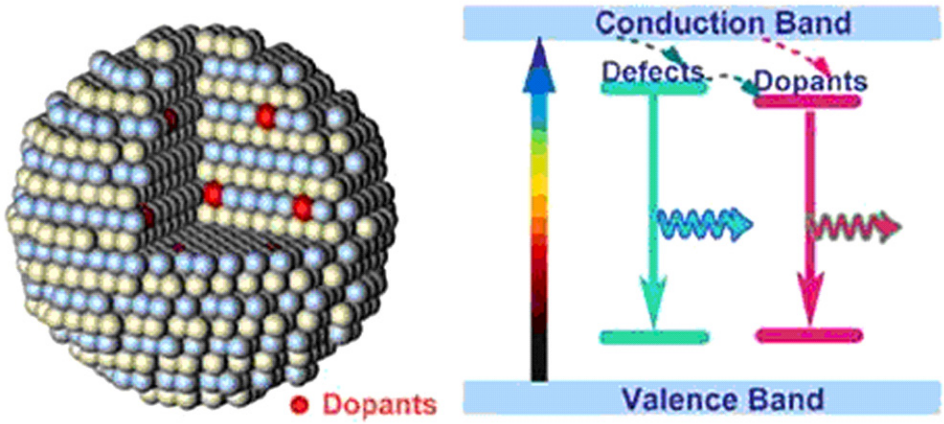

Scheme 1: *Schematic band-gap model for the luminescence of pure Sb_2S_3 and Ln^{3+} doped in Sb_2S_3.*

ions at 695 nm and by a strong absorption band in UV domain characteristic for Sb_2S_3. The energy level diagram is also proposed taking into account the optical absorption data of Loh [27] (Figure 10).

In case of $Sb_{1.91}Er_{0.09}S_3$, intra-4f Er^{3+} transitions of the $^4I_{11/2}$ and $^4I_{13/2}$ levels to the ground state ($^4I_{15/2}$) are expected around 1.54 µm. However, these can not be determined due to equipment limitations [28]. Figure 11 exhibits the RT PL emission spectra of Er^{3+} and Yb^{3+} in Sb_2S_3. Both the PL excitation spectra of Yb^{3+} and Er^{3+} are dominated by a strong UV broad band centered at 420 nm and 465 nm, respectively, which corresponds to the band-gap absorption peak of Sb_2S_3. Whereas, the emission spectra display the fingerprints of Yb^{3+} and Er^{3+} ions suggesting that the Yb^{3+} and Er^{3+} emissions could be achieved via an ET process from the Sb_2S_3 host to emitters. In this process, the Sb_2S_3 host serves as a light-harvesting antenna (i.e. sensitizer) to absorb UV excitation light and subsequently transferres energy to the dopants, resulting in the luminescence of the $^2F_{5/2}\rightarrow{}^2F_{7/2}$ transition of Yb^{3+} and the $^4I_{13/2}\rightarrow{}^4I_{15/2}$ transition of Er^{3+}. Emission of intra-4f Yb^{3+} transition is occured around 890 nm in addition to emission band of Sb_2S_3 lattice at 540 nm. But emission originating from Er^{3+} are occurred around 1540 nm and can not be seen due to equipment limitations[29,30]. Therefore, just emission of Sb_2S_3 related to Er-doped lattice with red shift in comparison to Sb_2S_3 are observed at 490 nm and 540 nm.

In doped semiconductors, two types of emissions are responsible for the dopant (impurity) luminescence. One can be observed only upon direct excitation of the dopant. The second type is obtained if energy transfer from host to dopant occurs. Scheme 1 shows band-gap model for the luminescence of pure and Ln^{3+} doped in Sb_2S_3.

Binary compounds such as Sb_2S_3 and its alloys are thermoelectric materials with small band gap and layered crystalline structures. These materials have been investigated for direct conversion of thermal energy to electric energy and they specially are using for electronic refrigeration [31,32]. The electerical resistivity of compounds is shown in

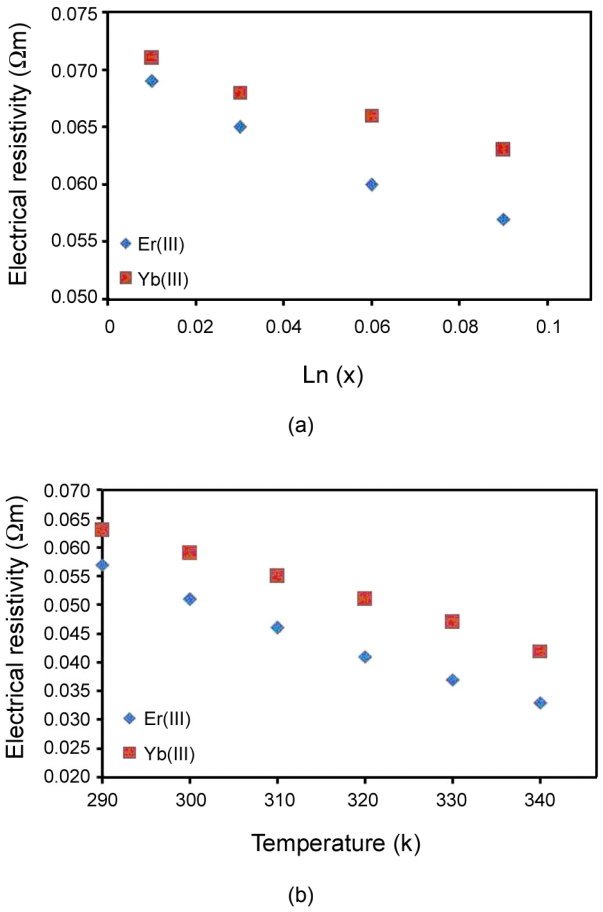

Figure 12: *Electerical (a) and Thermoelectrical (b) resistivity of $Sb_{2-x}Ln_xS_3$ (x = 0 to 0.09).*

Figure 12a. Increasing lanthanide cations concentration, the electrical resistivity of synthesized nano materials plumetted obviousely.In the case of Yb^{3+}-doped compounds the minimum value of electerical resistivity is 0.063 Ωm and about Er^{3+}-doped compounds is 0.057 Ωm. Also, the temperature dependence of the electrical resistivity for $Sb_{1.91}Er_{0.09}S_3$ and $Sb_{1.91}Er_{0.09}S_3$ between 290-340 K is shown in Figure 12b indicating that electrical resistivity decreases linearly with temperature. At room temperature the electrical resistivity of pure Sb_2S_3 was of the order of 0.1 Ω.m and in the case of $Sb_{1.91}Yb_{0.09}S_3$ and $Sb_{1.91}Er_{0.09}S_3$ were 6.3×10^{-2} Ω.m and 5.7×10^{-2} Ω.m, respectively. As a result, the electrical conductivity of doped-Sb_2S_3 are higher than pure Sb_2S_3 at room temperature and increase with

temperature. Between doped compounds, Er^{3+}-doped Sb_2S_3 has higher electrical conductivity than Yb^{3+}-doped Sb_2S_3.

4. CONCLUSIONS

Novel luminescent $Ln_xSb_{2-x}S_3$ (Ln: Er^{3+}, Yb^{3+}) based nanomaterials were synthesized by a simple and efficient co-reduction method at 48 h and 180°C at basic media. SEM images show that doping of Ln^{3+} into the sites of the Sb^{3+} results in different morphology. Emission spectra of Yb^{3+} doped materials, in addition to the characteristic red emission peaks of Sb_2Se_3 emission, show other bands originating very probably from the $^2F_{7/2} \rightarrow {}^2F_{5/2}$ in case of Yb^{3+} doped crystals. Rare earth doping improves the electrical conductivity of Sb_2S_3 dramatically as well as thermoelectrical conductivity. Due to the lower value for electrical conductivity in case of Yb^{3+}-doped nanoflowers, morphology has influence on electrical properties.

ACKNOWLEDGMENT

This study has been supported by the council of the university of Tabriz, Iran, and WCU nanoresearch center, South Korea.

REFERENCES

1. Sun Y., Chen Y., Tian L.J., Yu Y., Kong X.G., Zhang Y.L., Zhang H., *J. Lumin.*, **128**(2008), 15.
2. Tachikawa T., Ishigaki T., Li J., Fujitsuka M., Majima T., *Angew. Chem. Int. Ed.*, **47**(2008), 5348.
3. Wang F., Han Y., Lim C.S., Lu Y.H., Xu J., Chen H.Y., Zhang C., Liu X.G., *Nature*, **463**(2010), 1061.
4. Roy B., Chakraborty B.R., Bhattacharya R., Dutta A.K., *Solid. State. Commun.*, **25**(1978), 937.
5. Savadogo O., Mandal K.C., *Mat. Sol. C*, **26**(1992), 117.
6. Juarez B.H., Ibizate M., Palacios J.M., *Lopez, Adv. Mater.*, **15**(2003), 319.
7. N.K. Abrikosov, V.F. Bankina, L.V. Poretakaya, L.E. Shelimova, 1969. Semiconducting II-VI and V-VI Compounds, Plenum, New York, 1969.
8. Arivuoli D., Gnanam F.D., Ramasamy P., *J. Mater. Sci. Lett.*, **7**(1988), 711.
9. Rao C.N., Deepak F.L., Gundiah G., *Prog. Solid State Chem.*, **31**(2003), 5.
10. Geng Z.R., Wang M.X., Yue G.H., Yan P.X., *J. Cryst. Growth*, **10**(2008), 341.
11. Lalia-kantouri M., Marison A.G., Manoussakis G.E., *J. Therm. Anal.*, **29**(1984), 1151.
12. Alemi A., Joo S.W., Hanifehpour Y., Khandar A., Morsali A., *J. Nanomater.*, **2011**(2011), Article ID 186528.
13. Alemi A., Hanifehpour Y., Joo S.W., *J. Nanomater.*, **2011**(2011), Article ID 414798.
14. Yu Y., Wang R.H., Chen Q., Peng L.M., *J. Phys. Chem.*, **B109**(2005), 23312.
15. Patil N.S., Sargar A.M., Mane S.R., Bhosale P.N., *Appl. Surf. Sci.*, **254**(2007), 5261.
16. Augustin S., Mathai E., *Mater. Res. Bull.*, **36**(2001), 2251.
17. Lostak P., Drasar C., Klichova I., Cernohorsky T., *Phys. Status Solidi B*, **200**(1997), 289.
18. Janicek P., Drasar C., Lostak P., Vejpravova J., *Physica B*, **403**(2008), 3553.
19. Larson P., Lambrecht R.L., *Phys. Rev. B*, **78**(2008), 195207.
20. Gratens X., Isber S., Charar S., Fau C., Averous M., *Phys. Rev. B*, **55**(1997), 8075.
21. Alemi A., Babalou A., Dolatyari M., klein A., Meyer G., *Z. Anorg. Allg. Chem.*, **635**(2009), 2053.
22. Alemi A., Klein A., Meyer G., Dolatyari M., Babalou A., *Z. Anorg. Allg. Chem.*, **637**(2011), 87.
23. Alemi A., Hanifehpour Y., Joo S.W., Khandar A., Morsali A., Min B., *Physica B*, **406**(2011), 2801.
24. Alemi A., Hanifehpour Y., Joo S.W., Min B., *Physica B*, **406**(2011), 3831.
25. Alemi A., Hanifehpour Y., Joo S.W., Min B.,

Colloids and Surfaces A: Physicochem. Eng. Aspects, **390**(2011),142.
26. Alemi A., Hanifehpour Y., Joo S.W., Khandar A., Morsali A., B. Min, *Physica B*, **407**(2012), 38.
27. Loh E., *Phys. Rev.* **175**(1968) 533; *Loh E., Phys. Rev.*, **184**(1969), 348.
28. Ugolini C., Nepal N., Lin J.Y., Jiang H.X., *Appl. Phys. Lett.*, **90**(2007), 051110.
29. Strohheofer C., Polman A., *Opt. Mater.*, **21**(2003), 705.
30. Hoven G.N., Elsken J.A., Polman A., Dam C., Uffelen K., Smit M.K., *Appl. Optics,* **36**(1997), 3338.
31. Chim T., Chun B., *J. Alloys. Compd.*, **437**(2007), 225.
32. Ji H., Zhao X., Zhang, Lu B., Ni H., *Mater. Lett.*, **59**(2005), 682.